

M. Mattioli, M.E. Puiatti, M. Valisa, I. Coffey, R. Dux, P. Monier-Garbet,  
M.F.F. Nave, J. Ongena, M. Stamp, J. Strachan and M.von Hellermann

# Simulation of the Time Behavior of Impurities in JET Ar-Seeded Discharges and its Relation with Sawteething



# Simulation of the Time Behavior of Impurities in JET Ar-Seeded Discharges and its Relation with Sawteething

M. Mattioli<sup>1</sup>, M.E. Puiatti<sup>1</sup>, M. Valisa<sup>1</sup>, I. Coffey<sup>2</sup>, R. Dux<sup>3</sup>, P. Monier-Garbet<sup>4</sup>, M.F.F. Nave<sup>5</sup>, J. Ongena<sup>6</sup>, M. Stamp<sup>7</sup>, J. Strachan<sup>8</sup>, M.von Hellermann<sup>9</sup>  
and contributors to the EFDA-JET workprogramme\*

<sup>1</sup>*Consorzio RFX, Associazione Euratom-ENEA sulla Fusione, Padova, Italy*

<sup>2</sup>*Queens University, Belfast BT7 INN, North Ireland*

<sup>3</sup>*Max-Planck Institut für Plasmaphysik, EURATOM Association, D-8046 Garching, Germany*

<sup>4</sup>*Association Euratom-CEA, DRFC, CEA Cadarache, St Paul lez Durance, France*

<sup>5</sup>*Associação Euratom-IST, Centro de Fusão Nuclear, Lisboa, Portugal*

<sup>6</sup>*LPP-ERM/KMS Euratom-Belgian State Association, Brussels, Belgium*

<sup>7</sup>*EURATOM/UKAEA Fusion Association, Culham Science Center, Abingdon, Oxon. UK*

<sup>8</sup>*Princeton Plasma Physics Laboratory, USA*

<sup>9</sup>*FOM Instituut voor Plasmafysica Rijnhuizen, EURATOM Association, Nieuwegein, The Netherlands*

“This document is intended for publication in the open literature. It is made available on the understanding that it may not be further circulated and extracts or references may not be published prior to publication of the original when applicable, or without the consent of the Publications Officer, EFDA, Culham Science Centre, Abingdon, Oxon, OX14 3DB, UK.”

“Enquiries about Copyright and reproduction should be addressed to the Publications Officer, EFDA, Culham Science Centre, Abingdon, Oxon, OX14 3DB, UK.”

## INTRODUCTION

In previous papers the behaviour of impurities and radiation in JET Ar seeded Elmy H-mode discharges, in which the plasma reaches high confinement values at densities close or even exceeding the Greenwald limit has been studied [1, 2]. The impurity transport with different magnetic configurations and heating schemes has been analyzed in the so called ‘after-puff phase’ (AP), which is the period featuring good confinement properties that follows the phase of a strong Ar and D2 puffing (‘inflow phase’, IP). The aim of this paper is a more detailed simulation of the time behaviour of Ar and C (that is the main intrinsic impurity in JET), starting from the IP up to the evolution during the AP. The soft X-rays inverted profiles, now available, allow a better determination of the convective velocity and diffusion coefficient profiles, and a more detailed time analysis of the impurities.

## THE EXPERIMENTS

Two types of discharges, characterized by different Ar transport regimes, are compared. In the first one (Pulse No: 52136,  $B_t = 2.5$  T,  $I_p = 2.5$  MA,  $q_{95} = 3.05$ ) the plasma is heated by 12 MW NB only. In the second one (Pulse No: 52146, with  $B_t = 2.6$  T,  $I_p = 2.7$  MA,  $q_{95} = 3.05$ ) 2 MW of ICRH added to NB help maintaining some level of sawtooth (ST) activity. Both discharges refer to a septum configuration, i.e. the X point is on the dome of the divertor, at low triangularity (0.25 lower triangularity, 0.18 upper triangularity). The main plasma parameters during the IP and the AP are drawn in Fig.1.

In fig.2 the Abel inverted on-axis soft X-rays (SXR) emissivity shows a ST inversion between the inflow and the after-puff phase: at the ST crash the SXR signal increases during the IP and, on the contrary, decreases during the AP. As it will be discussed in the following, the first condition corresponds to Ar penetration in the plasma centre, the second one to Ar expulsion from the core. The simulations reported are based on a 1D impurity transport model coupled to a collisional-radiative model [3]. The Ar influx (boundary condition to the code) is determined by reproducing an Ar XV line evolution. The radial impurity ion flux  $\Gamma_Z(r)$  is expressed as the sum of a diffusive and convective term:

$$\Gamma_Z(r) = -D(r) \partial n_Z(r) / \partial r + v(r) n_Z(r).$$

where  $n_Z$  indicates the density of the ion of charge  $(Z-1)$ ,  $D$  is the diffusion coefficient and  $v$  the pinch velocity ( $v > 0$  corresponds to outward velocity).

## THE ARGON INFLOW PHASE

The two discharges do not show great differences in this phase. A good simulation of Ar can be obtained with the same transport parameters, drawn in Fig.3. The diffusion coefficient in the external half of the plasma is  $0.8 \text{ m}^2/\text{s}$ , decreasing to  $0.15 \text{ m}^2/\text{s}$  in the centre (about 3 times the neoclassical value), with a region at low diffusivity at  $r/a \geq 0.95$ , as found also from the previous simulations of the JET spectra [3] during AP.

For carbon, to reproduce the high experimental value of the ratio  $r$  between the  $\text{Ly}\alpha$   $33.7\text{\AA}$  C VI brightness and the resonance  $40.2\text{\AA}$  C V line ( $\rho \sim 4$ ) the edge diffusion barrier assumed for Ar is not sufficient: an higher inward velocity in the last 0.2m of the plasma radius has to be prescribed. The radial profiles of the total Ar and C density and of the SXR emissivity at the end of the IP are shown for both discharges in Fig.4(a) and 4(b), respectively. It can be observed that in this phase the impurity profiles are hollow (both Ar and C).

The ST have been simulated assuming in the calculation a discontinuity in the temperature profile (decreased by 200eV on the axis) and in the diffusion coefficient (increased up to  $50\text{m}^2/\text{s}$  in the central region). The enhanced diffusion implies a flattening of the Ar density profile. Since the latter is hollow before the crash, its flattening corresponds to a progressive entrance of Ar in the plasma core at each ST crash, since the contribution due to the enhancement of the central diffusion dominates on the effect of the decreased temperature. The simulated and experimental SXR profiles in correspondence with a ST and just before it are shown in Fig.5

### THE AFTER-PUFF PHASE

Experimentally, differences are observed in the impurity behavior between the two analyzed discharges. In Pulse No: 52136 Ar accumulates in the plasma centre, as shown by the progressive peaking of the radiated power and of the SXR emission profiles and by the  $\text{Ar}^{18+}$  CX data. The transport parameters determined by the simulation of the AP are shown in fig.6: the diffusion coefficient is the same allowing the simulation of the IP, while the pinch velocity in the central region is inward. It has to be mentioned that the characteristics of the  $D$  and  $v$  profiles are the same as found in [1], except for the inward pinch velocity, that in the central region has been found to be lower by a factor of about 2. This reconstruction has to be considered as more reliable, as it is based on the reproduction of the inverted SXR profiles. On the contrary, in Pulse No: 52146 the profiles of SXR,  $\text{Ar}^{18+}$  and radiated power are not as peaked as in Pulse No: 52136, and consequently to reproduce the experimental data a quite lower inward pinch velocity is required (Fig.6). Figure 7 compares the total Ar and the  $\text{Ar}^{18+}$  density and the SXR profiles obtained from the simulations of the two discharges in between two ST. The experimental CX data and Abel inverted SXR profiles are also shown.

For carbon the transport coefficients do not change with respect to the IP in both discharges and also in this phase the simulation of the line spectra leads to different external transport barriers for C and Ar.

An open question is to what extent the different behaviour of these two discharges in terms of Ar accumulation in the plasma centre is associated with the maintenance of ST when ICRH keeps the safety factor  $q(0)$  just around 1. In fact in this phase the density profiles of Ar high-Z ions are peaked, and the enhanced diffusion corresponding to the ST crash has a flattening effect that results in an “expulsion” of Ar [2]. This process can be observed in Fig.2 as the decrease of central SXR emissivity (combined effect of Ar flattening and  $T_e$  decrease) corresponding to the ST crashes. To

simulate the evolution of the SXR profiles at the ST crash (fig.8), besides a sudden increase of the diffusion coefficient a higher outward velocity has to be prescribed in the centre, accompanied by the decrease of  $T_e$ . The ST flattens slightly the SXR profile that recovers before the subsequent ST crash, about 0.35s after. The global influence of ST on the Ar density profiles can be inferred from Fig.9, which shows the density at 3.3s obtained with and without the inclusion in the calculation of 3 ST in the AP phase. Though not in a dramatic way, ST have a direct influence on the Ar density profile evolution, and are likely to play a role in maintaining the profiles stationary, their expulsion mechanism competing against the accumulation in the core.

## **CONCLUSION**

The time evolution of C and Ar has been simulated in two Ar-seeded high performance JET discharges, with and without Ar accumulation during the after-puff phase, respectively. The inflow phase has been well simulated with the same transport coefficient profiles for both discharges, while during the AP the non-accumulating discharge required a lower inward pinch velocity. The analysis of ST during the AP of the non-accumulating discharge has indicated that they contribute to the Ar accumulation avoidance, in conjunction with a central transport regime already characterized by relatively low inward pinch velocity.

## **REFERENCES**

- [1]. Puiatti et al. . 2001, ECA vol.25A, ( Madeira, EPS 2001) p.933 (paper P3.007)
- [2]. Nave M.F.F. et al. 2001, ECA VOL.25A (Madeira, EPS 2001) p.961 (paper P3.009)
- [3]. Mattioli M., et al., Plasma Phys. Control. Fus.**44** (2002) 33

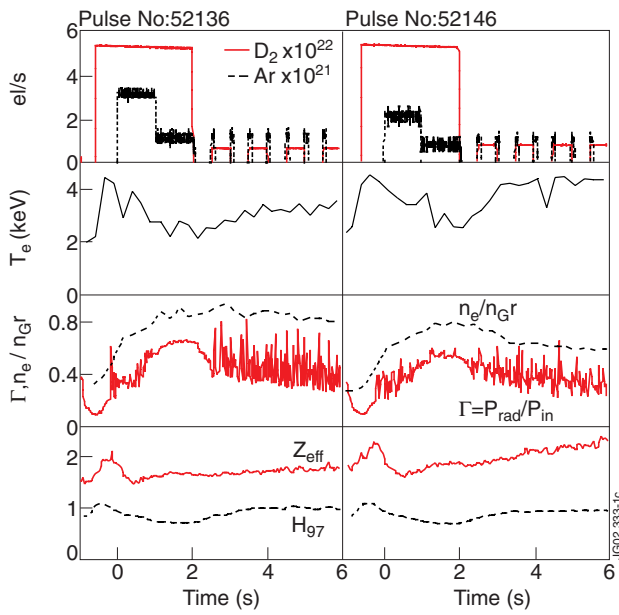


Figure 1:

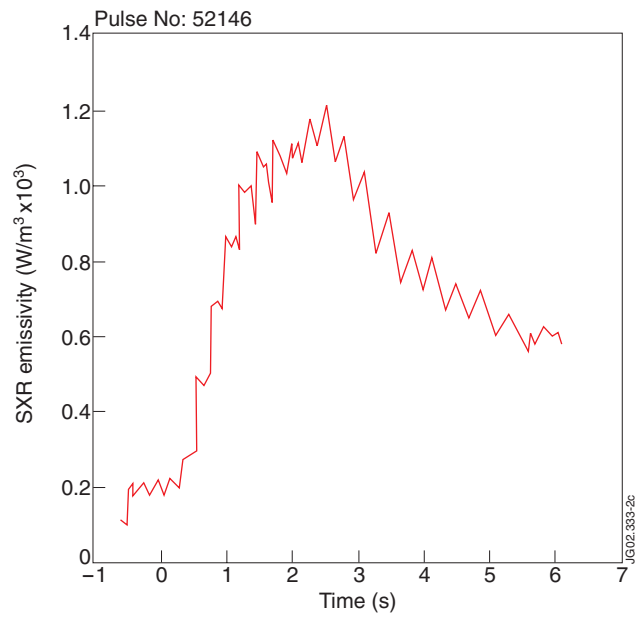


Figure 2:

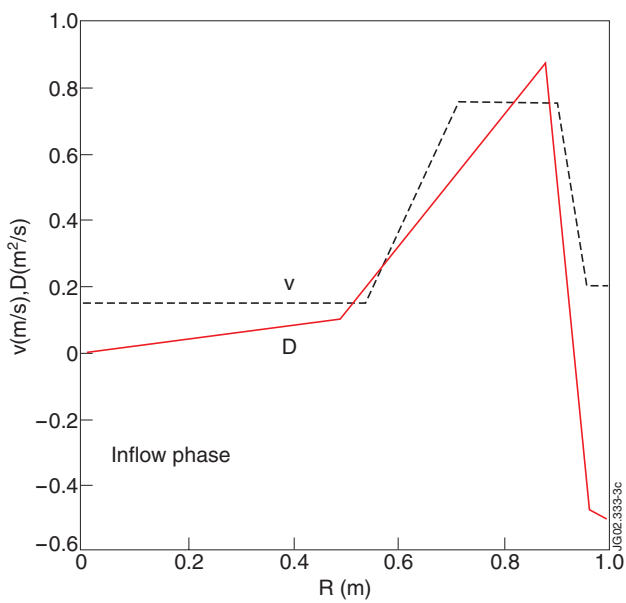


Figure 3:

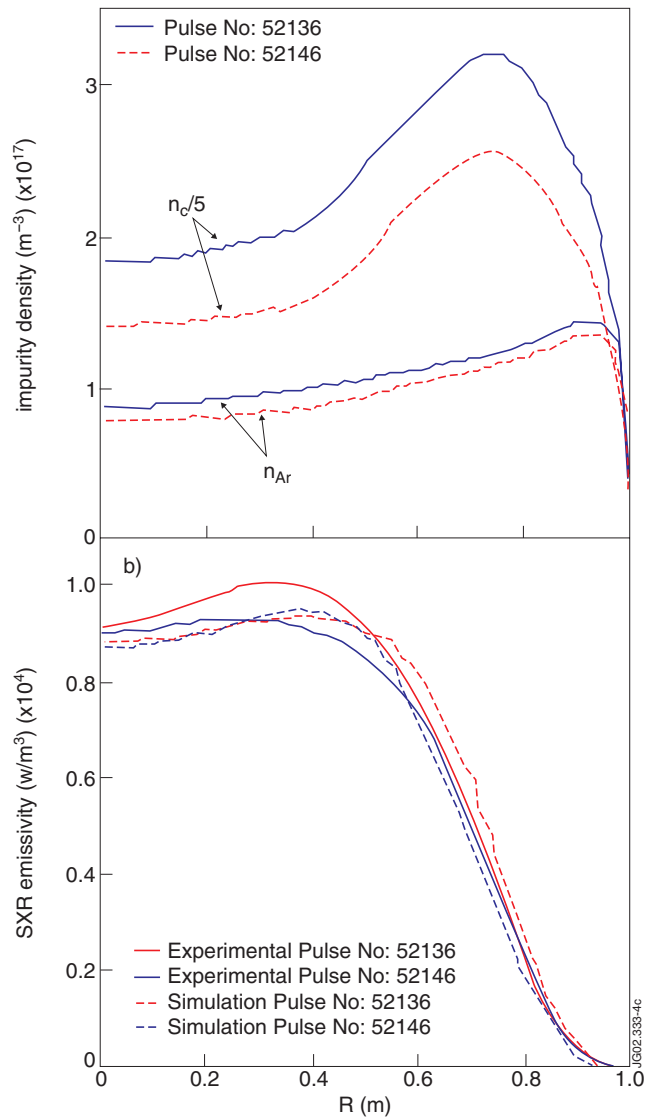


Figure 4:



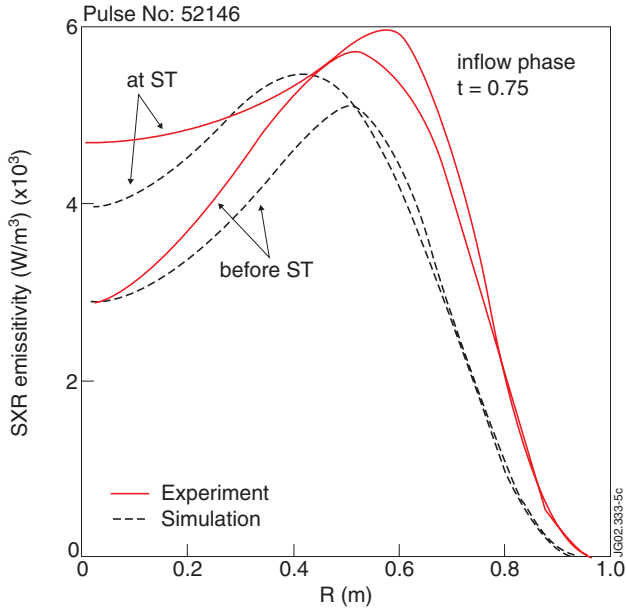


Figure 5:

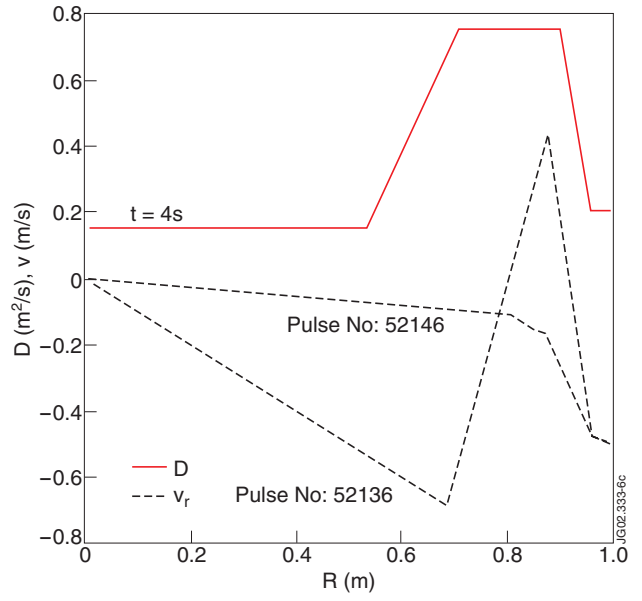


Figure 6:

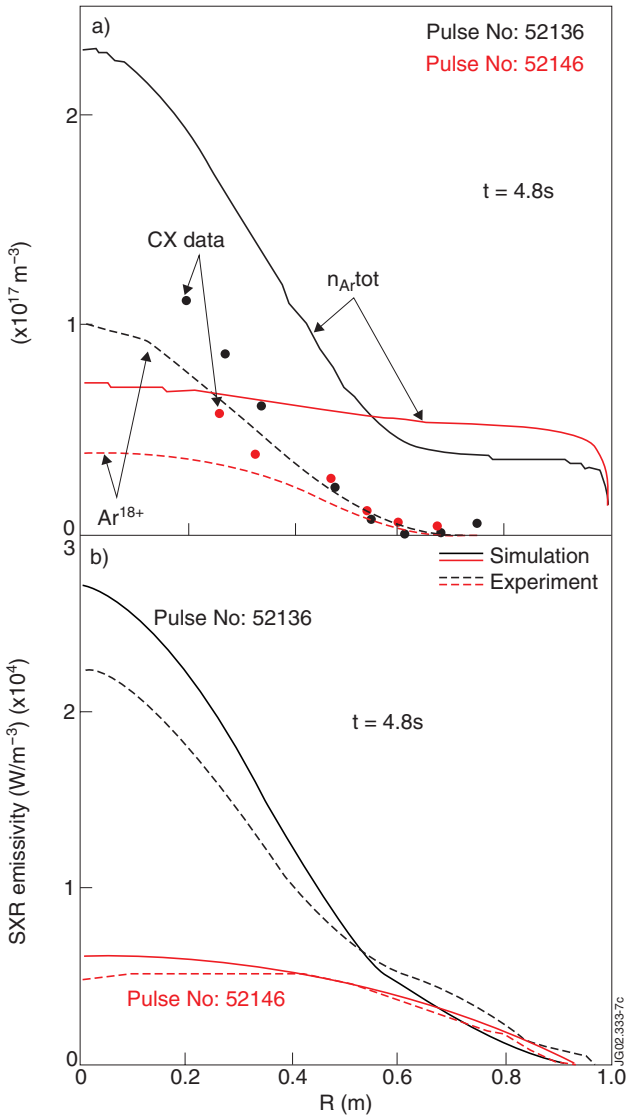


Figure 7:

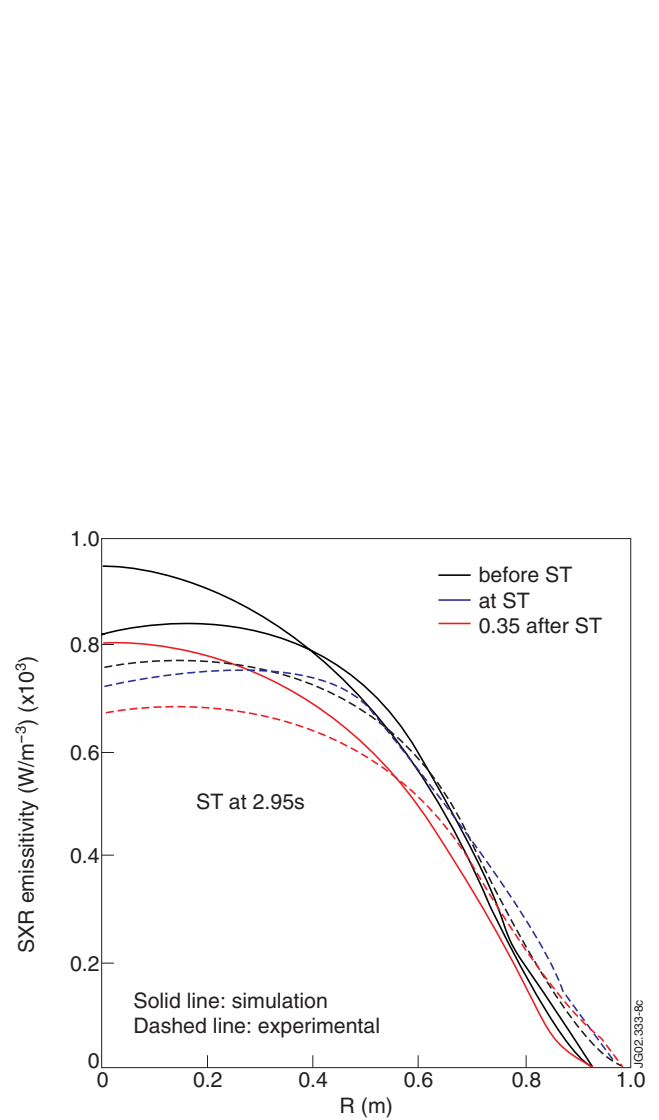


Figure 8:

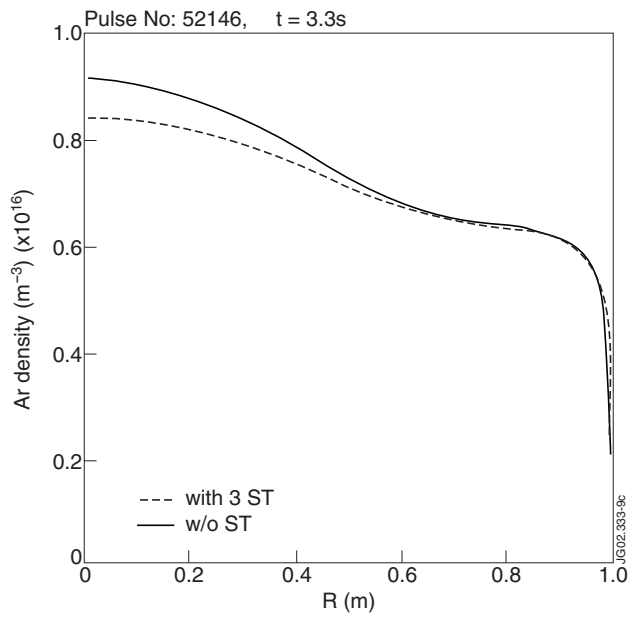


Figure 9: